1 **Title**: Geometrical model explains multiple preferred escape trajectories of fish

2 **Short title**: Geometrical model for escape trajectories

3 **Author affiliations**:

4 Yuuki Kawabata[a,*], Hideyuki Akada[b], Ken-ichiro Shimatani[c], Gregory N. Nishihara[d], Hibiki Kimura[a],

5 Nishiumi Nozomi[a,e], Paolo Domenici[f]

6 [a]*Graduate School of Fisheries and Environmental Sciences, Nagasaki University, 1-14 Bunkyo-machi,*

7 *Nagasaki 852-8521, Japan*

8 [b]*Faculty of Fisheries, Nagasaki University, 1-14 Bunkyo-machi, Nagasaki 852-8521, Japan*

9 [c]*The Institute of Statistical Mathematics, 10-3 Midori-cho, Tachikawa, Tokyo 190-8562, Japan*

10 [d]*Institute for East China Sea Research, Organization for Marine Science Technology, Nagasaki*

11 *University, 1551-7 Taira-machi, Nagasaki 851-2213, Japan*

12 [e]*National Institute for Basic Biology, 5-1 Higashiyama, Myodaiji, Okazaki, Aichi 444-8787, Japan.*

13 [f]*CNR-IAS, Località Sa Mardini, 09170, Torregrande, Oristano, Italy*

14 ***Corresponding author**: Yuuki Kawabata

15 Email: yuuki-k@nagasaki-u.ac.jp; Tel: +81-(0)95-819-2824

16

17 **Author contributions:** Y.K. conceived the study; Y.K. and P.D. constructed the theoretical model; Y.K.
18 and H.A. designed the experiment, Y.K., H.A., H.K., and N.N. conducted the experiment; H.A. and
19 H.K. digitized the videos; Y.K., K.S., G.N.N., and P.D. conducted statistical analyses; Y.K. wrote the
20 manuscript with input from K.S., G.N.N., N.N., and P.D.

21 **Keywords**: escape direction; escape response; escape turn; mathematical model; predator evasion

22

Abstract

To evade predators, many prey perform rapid escape movements. The resulting escape trajectory (ET) – measured as the angle of escape direction relative to the predator's approach path – plays a major role in avoiding predation. Previous geometrical models predict a single ET; however, many animals (fish and other animal taxa) show highly variable ETs with multiple preferred directions. Although such a high ET variability may confer unpredictability, preventing predators from adopting counter-strategies, the reasons why animals prefer specific multiple ETs remain unclear. Here, we constructed a novel geometrical model in which T_{diff} (the time difference between the prey entering the safety zone and the predator reaching that entry point) is expected to be maximized. We tested this prediction by analyzing the escape responses of *Pagrus major* attacked by a dummy predator. At each initial body orientation of the prey relative to the predator, our model predicts a multimodal ET with an optimal ET at the maximum T_{diff} ($T_{\mathrm{diff,1}}$) and a suboptimal ET at a second local maximum of T_{diff} ($T_{\mathrm{diff,2}}$). Our experiments show that when $T_{\mathrm{diff,1}}-T_{\mathrm{diff,2}}$ is negligible, the prey uses optimal or suboptimal ETs to a similar extent, in line with the idea of unpredictability. The experimentally observed ET distribution is consistent with the model, showing two large peaks at 110–130° and 170–180° away from the predator. Because various animal taxa show multiple preferred ETs similar to those observed here, this behavioral phenotype may result from convergent evolution that combines maximal T_{diff} with a high level of unpredictability.

Significance Statement

Animals from many taxa escape from suddenly approaching threats, such as ambush predators, by using multiple preferred escape trajectories. However, the reason why these multiple preferred escape trajectories are used is still unknown. By fitting a newly constructed model to the empirical escape response data, we show that the seemingly complex multiple preferred escape trajectories can arise from a simple geometrical rule which maximizes the time difference between when the prey enters the safety zone and when the predator reaches that entry point. Our results open new avenues of investigation for understanding how animals choose their escape trajectories from behavioral and neurosensory perspectives.

Introduction

When exposed to sudden threatening stimuli such as ambush predators, many prey initiate escape responses that include turning swiftly and accelerating away from the threat. The escape responses of many invertebrate and lower vertebrate species are controlled by giant neurons that ensure a short response time (1). Many previous studies have focused on two behavioral traits that are fundamental for avoiding predation: when to escape (i.e., flight initiation distance, which is measured as the distance from the predator at the onset of escape) and where to escape [i.e., escape trajectory (ET), which is measured as the angle of escape direction relative to the stimulus direction] (2). Previous studies have investigated the behavioral and environmental contexts affecting these variables (3-8), because they largely determine the success or failure of predator evasion (9-13), and hence the fitness of the prey species. A large number of models on how animals determine their flight initiation distances have been formulated and tested by experiments (2). Although a number of models have also been developed to predict animal ETs (4, 14, 15), there are still some unanswered questions about how the variability of the observed ETs is generated.

Previous geometrical models predict a single ET that depends on the relative speeds of the predator and the prey (4, 14, 15). However, these simple models do not explain the complex ET distributions reported in empirical studies on various taxa of invertebrates and lower vertebrates (reviewed in ref. 16). Whereas some animals exhibit unimodal ET patterns that satisfy the geometrical models (e.g., ref. 17), many animals show multimodal ETs within a limited angular sector (esp., 90–

71 180°) (e.g., ref. 4, 5, 18). To explore the discrepancy between the predictions of the models and
72 empirical data, some researchers have hypothesized mechanical/sensory constraints (16, 19) and
73 unpredictability, in line with the idea of a protean response that does not allow predators to adopt
74 counter-strategies (19-21). Although these hypotheses, together with the previous geometrical models,
75 can explain the ET variability within a limited angular sector, the reasons why animals prefer specific
76 multiple ETs still remain unclear.

77 In previous geometrical models, the prey was assumed to instantaneously escape in any
78 direction, irrespective of the prey's initial body orientation relative to the predator's approach path
79 (hereafter, initial orientation) (4, 14, 15). However, additional time is required for the change of the
80 heading direction (i.e. turn), therefore a realistic model needs to take into account that the predator can
81 approach the prey more closely while the prey is turning (12). Additionally, in previous models,
82 attacking predators were assumed to move for an infinite distance at a constant speed (4, 14, 15).
83 However, the attacks of many real predators, especially ambush ones, end at a certain distance from
84 initial positions of the prey (22-24). Therefore, we constructed a geometrical model that incorporates
85 two additional factors: the time required for the prey to turn and the endpoint of the predator attack.
86 We tested whether our model could predict empirically observed multimodal ETs, using the escape
87 response of the prey fish *Pagrus major* against an approaching dummy predator. The biological
88 implications resulting from the model and experimental data are then discussed within the framework
89 of predator–prey interactions.

Model

We revised a previous model proposed by Domenici (15, 25) (Fig. 1A). Other previous models (4, 14) made predictions that were similar to those of Domenici's model although they used different theoretical approaches. In Domenici's model, the predator with a certain width (i.e. the width of a killer whale's tail used as a weapon to catch prey) directly approaches the prey, and the prey (the whole body) should enter the safety zone before the predator reaches that entry point. In this model, the prey can instantaneously escape in any direction, and the predation threat moves linearly and infinitely.

In our new model (Fig. 1B), two factors are added to Domenici's model: the time required for the prey to turn and the endpoint of the predator attack. We assume that a prey with a certain initial orientation β (spanning 0–180°, where 0° and 180° correspond to being attacked from front and behind, respectively) evades a sudden predation threat. The edges of the safety zone are determined by the width of the predator gape D_{width}, and the distance between the prey's initial position and the predator's mouth position at the end of the predator attack D_{attack}. This model is based on the escape response of the horizontal plane, which is realistic for many fish species as well as invertebrate species that walk on substrates. Startled fish respond to the attack by turning at an angle α, and the ET results from the angular sum of α and β. ETs from the left and right sides were pooled and treated as though they were stimulated from the right side (Fig. S1; See "Definition of Angles" in Materials and Methods section for details).

The prey can escape from the predator when the time required for the prey to enter the safety zone (T_{prey}) is shorter than the time required for the predator's mouth to reach that entry point (T_{pred}). Therefore, the prey is assumed to optimize the difference between the T_{pred} and T_{prey} (T_{diff}). To incorporate the time required for the prey to turn, T_{prey} was divided into two phases: the fast-start phase, which includes the time for turning and acceleration (T_1), and the constant speed phase (T_2). This assumption is consistent with the previous studies (26-28) and was supported by our experiment (See Fig. S3). Therefore:

$$T_{\text{prey}} = T_1 + T_2 \quad [1]$$

For simplicity, the fish was assumed to end the fast-start phase at a certain displacement from the initial position in any α (D_1; the radius of the dotted circle in Fig. 1B) and to move at a constant speed U_{prey} to cover the rest of the distance (toward the edge of the safety zone D_2, plus the length of the body that is posterior to the center of mass L_{prey}). Because a larger $|\alpha|$ requires further turning prior to forward locomotion, which takes time (26, 29), and the initial velocity after turning was dependent on $|\alpha|$ in our experiment (See Fig. 3B), T_1 is given by a function of $|\alpha|$ [$T_1(|\alpha|)$]. Therefore, T_{prey} can be expressed as:

$$T_{\text{prey}} = T_1(|\alpha|) + \frac{D_2}{U_{\text{prey}}} + \frac{L_{prey}}{U_{\text{prey}}} \quad [2]$$

T_{pred} can be expressed as:

$$T_{\text{pred}} = \frac{D_3 + D_{\text{initial}}}{U_{\text{pred}}} \quad [3]$$

where D_3 is the projection of the prey's escape path along the edge of the sideways safety zone, D_{initial} is the distance between the prey and the predator at the onset of the prey's escape response (i.e., the flight initiation distance or reaction distance), and U_{pred} is the predator speed, which is assumed to be constant. From equations [2] and [3], T_{diff} can be calculated as:

$$T_{\text{diff}} = \frac{D_3}{U_{\text{pred}}} + \frac{D_{\text{initial}}}{U_{\text{pred}}} - T_1(|\alpha|) - \frac{D_2}{U_{\text{prey}}} - \frac{L_{prey}}{U_{\text{prey}}} \quad [4]$$

The ET toward the upper-left corner of the rectangular danger zone is calculated as $180 - \arctan(\frac{D_{\text{width}}}{2D_{\text{attack}}})$ (°), and thus D_2 and D_3 can be expressed as:

$$D_2 = \begin{cases} \dfrac{D_{\text{width}}}{2\sin(\alpha+\beta)} - D_1, \alpha+\beta < 180 - \arctan\left(\dfrac{D_{\text{width}}}{2D_{\text{attack}}}\right) \\ \dfrac{D_{\text{attack}}}{\cos(180-\alpha-\beta)} - D_1, \alpha+\beta \geq 180 - \arctan(\dfrac{D_{\text{width}}}{2D_{\text{attack}}}) \end{cases} \quad [5]$$

$$D_3 = \begin{cases} \dfrac{D_{\text{width}}\tan(\alpha+\beta-90)}{2}, \alpha+\beta < 180 - \arctan\left(\dfrac{D_{\text{width}}}{2D_{\text{attack}}}\right) \\ D_{\text{attack}}, \alpha+\beta \geq 180 - \arctan(\dfrac{D_{\text{width}}}{2D_{\text{attack}}}) \end{cases} \quad [6]$$

From equations [4], [5], and [6],

$$T_{\text{diff}} = \begin{cases} \dfrac{D_{\text{width}}\tan(\alpha+\beta-90)}{2U_{\text{pred}}} - \dfrac{D_{\text{width}}}{2U_{\text{prey}}\sin(\alpha+\beta)} - T_1(|\alpha|) - \dfrac{D_1}{U_{\text{prey}}} + \dfrac{D_{\text{initial}}}{U_{\text{pred}}} - \dfrac{L_{prey}}{U_{\text{prey}}}, \alpha+\beta < 180 - \arctan(\dfrac{D_{\text{width}}}{2D_{\text{attack}}}) \\ \dfrac{D_{\text{attack}}}{U_{\text{pred}}} - \dfrac{D_{\text{attack}}}{U_{\text{prey}}\cos(180-\alpha-\beta)} - T_1(|\alpha|) - \dfrac{D_1}{U_{\text{prey}}} + \dfrac{D_{\text{initial}}}{U_{\text{pred}}} - \dfrac{L_{prey}}{U_{\text{prey}}}, \alpha+\beta \geq 180 - \arctan(\dfrac{D_{\text{width}}}{2D_{\text{attack}}}) \end{cases} \quad [7]$$

Because the terms $\frac{D_1}{U_{\text{prey}}}$, $\frac{D_{\text{initial}}}{U_{\text{pred}}}$, and $\frac{L_{prey}}{U_{\text{prey}}}$ are independent of α and β, we can calculate the relative values of T_{diff} (T_{diff}') in response to the changes of α and β, from D_{width}, D_{attack}, U_{prey}, U_{pred}, and $T_1(|\alpha|)$ as:

$$T'_{\mathrm{diff}} = \begin{cases} \dfrac{D_{\mathrm{width}} \tan(\alpha+\beta-90)}{2U_{\mathrm{pred}}} - \dfrac{D_{\mathrm{width}}}{2U_{\mathrm{prey}} \sin(\alpha+\beta)} - T_1(|\alpha|), \alpha+\beta < 180 - \arctan\left(\dfrac{D_{\mathrm{width}}}{2D_{\mathrm{attack}}}\right) \\ \dfrac{D_{\mathrm{attack}}}{U_{\mathrm{pred}}} - \dfrac{D_{\mathrm{attack}}}{U_{\mathrm{prey}} \cos(180-\alpha-\beta)} - T_1(|\alpha|), \alpha+\beta \geq 180 - \arctan\left(\dfrac{D_{\mathrm{width}}}{2D_{\mathrm{attack}}}\right) \end{cases} \quad [8]$$

Given that the escape success is assumed to be dependent on T_{diff}', the theoretically optimal ET can be expressed as:

$$\text{The optimal ET} = \underset{\alpha+\beta}{\operatorname{argmax}}(T_{\mathrm{diff}}') \quad [9]$$

Results

Experimental Results

P. major exhibited a typical C-start escape response (Fig. S1), which consists of the initial bend (stage 1), followed by the return tail flip (stage 2), and continuous swimming or coasting (stage 3) (30, 31). Figure 2 shows the effect of the initial orientation β on the ETs. As was done in previous studies (16, 32, 33), the away (contralateral) and toward (ipsilateral) responses, defined as the first detectable movement of the fish oriented either away from or toward the predator, were analyzed separately. When the initial orientation was small (i.e., the prey was attacked head-on; Fig. 2A; $0° \leq \beta < 30°$), two peaks in the ET distribution were observed: a larger peak at around 100° (away response) and a smaller one at around −80° (toward response). As the initial orientation increases (Fig. 2A; $30° \leq \beta < 60°$), the peak at around −80° disappeared. As the initial orientation further increases beyond 60°, another peak appeared at around 170° (Fig. 2A). When the initial orientation was large (i.e., the prey was attacked from behind; Fig. 2A; $150° \leq \beta \leq 180°$), there were two similar-sized peaks in the ET at around 130°

(toward response), and 180–200° (away response). There were significant effects of initial orientation on the ET in both the away and the toward responses [away: generalized additive mixed model (GAMM), F=214.81, P<0.01; toward: GAMM, F=373.92, P<0.01]. There were significant effects of initial orientation on the turn angle α in away and toward responses (Fig. S2; away: GAMM, F=90.88, P<0.01; toward: GAMM, F=42.48, P<0.01). In the overall frequency distribution of ETs pooling the data on all initial orientations and both toward and away responses, there were two large peaks at 120–130° and 170–180°, and one small peak at around −80° (Fig. 2C). These 3 peaks were confirmed by the Gaussian mixture model analysis (34), where we fitted 1–9 Gaussian curves to the ETs, and selected the most parsimonious model based on the Akaike Information Criterion (AIC) (Table S1).

There were no significant effects of predator speed on the ET and $|\alpha|$ in either the toward or the away responses (ET, away: GAMM, F=0.01, P=0.93; ET, toward: GAMM, F=0.05, P=0.82; $|\alpha|$, away: GAMM, F=0.01, P=0.93; $|\alpha|$, toward: GAMM, F=0.05, P=0.82). There were no significant effects of predator speed [slow (from the minimum to the 33.3% quantile): 0.13~0.93 m/s; and fast (from the 66.7% quantile to the maximum): 1.29~1.88 m/s] on the variations of ETs and $|\alpha|$ in all 30° initial orientation bins (Levene's test, W=0.01~3.57, P=0.07~0.91).

Parameter Estimation

The distance of the fast-start phase (D_1) was regarded as 15 mm based on the relationship between displacement and velocity of the prey in the experiments (Fig. S3), where the velocity increased up to

about 15 mm of displacement from the initial position, beyond which it plateaus; over the 15 mm displacement from the initial position, there were no significant differences in the mean velocity between any combinations of 3-mm intervals in any 30° $|\alpha|$ bins (Fig. S3; paired *t*-test with Bonferroni's correction, $P>0.05$). There were significant effects of $|\alpha|$ on the time for a displacement of 15 mm from the initial position (GAMM, $F=70.31$, $P<0.01$) and on the mean velocity during the displacement (GAMM, $F=69.49$, $P<0.01$). However, there were no significant effects of $|\alpha|$ on the time required for a displacement of 15 to 30 mm from the initial position (GAMM, $F=1.52$, $P=0.22$) and on the mean velocity during the displacement (GAMM, $F=0.89$, $P=0.27$). Therefore, the time required for the prey to turn was incorporated into the model by analyzing the relationship between $|\alpha|$ and the time required for a displacement of 15 mm. The mean velocity of the prey during the constant phase U_{prey} was estimated to be 1.04 m s^{-1}, based on the experimental data. Because the cut-off distance might affect the overall results of the study, we have repeated all the statistical analyses (See Tables 1, 2, and the text below for results with a cut-off distance of 15 mm) with cut-off distances of 10 and 20 mm and confirmed that the overall results are insensitive to the changes (Tables S2 and S3).

The relationship between $|\alpha|$ and the time required for a displacement of 15 mm, $T_1(|\alpha|)$, is shown in Fig. 3. The time was constant up to 44° of $|\alpha|$, above which the time linearly increased in response to the increase of $|\alpha|$ (Fig. 3A). In the hierarchical Bayesian model, the lowest widely applicable or Watanabe-Akaike information criterion (WAIC) was obtained for the piecewise linear regression model (Table 1). To understand the possible mechanism of the relationship, the relationship

198 between $|\alpha|$ and initial velocity after a stage 1 turn, calculated as the displacement per second during
199 the 10 milliseconds (ms) after the turn, was also evaluated (Fig. 3B). The velocity increased in response
200 to $|\alpha|$ up to 46°, beyond which it plateaus. In the hierarchical Bayesian model, the lowest WAIC was
201 obtained for the piecewise linear regression model (Table 1). In both relationships, the regression lines
202 by the piecewise linear model were similar to those by the GAMM, suggesting that the general trends
203 of the relationships were clearly captured by this method. The change points of the two relationships
204 were not significantly different [difference: 1.70±18.01° (mean±95% Bayesian credible intervals)].
205 These results indicate that fish with a small $|\alpha|$ (<<45°) can accomplish the stage 1 turn quickly but
206 their velocity after the turn is lower, while fish with an intermediate $|\alpha|$ (=45°) spend a longer time on
207 the stage 1 turn, but their velocity after the turn is higher. Fish with a large $|\alpha|$ (>> 45°) spend a still
208 longer time on the stage 1 turn, but their velocity after the turn is similar to that with an intermediate
209 $|\alpha|$ (Fig. 3).

210 Because we have no previous knowledge about the values of U_{pred} and D_{attack} that the prey
211 regards as dangerous, we have optimized the values from the perspective of the prey using the
212 experimental data (See Materials and Methods for details). Briefly, the optimal values for prey were
213 obtained using the ranking index, where 0 means that the real fish chose the theoretically optimal ET
214 where T_{diff} is the maximum, and 1 means that the real fish chose the theoretically worst ET where T_{diff}
215 is the minimum (e.g., going toward the predator). The result shows that the optimal value of D_{attack} is
216 35.29 mm and the optimal value of U_{pred} is 1.34 m s^{-1}. Using data from previously published predator-

prey experiments on the same species of prey and predator (12), we show that the estimated D_{attack} value is at the upper limit of the empirical data and the estimated U_{pred} value is higher than the mean of the observed predator speed (Fig. S4). These results suggest that the values independently estimated in the present study are reasonable, and the prey chooses the ETs by estimating the values of D_{attack} and U_{pred} to be higher than their means used by the real predator, likely because an unsuccessful escape can result in death or severe injury.

Comparison of Model Predictions and Experimental Data

Figure 4A plots the relationships between the ET and the relative time difference T_{diff} for different initial orientations β, estimated by the geometrical model; Fig. 4B plots the relationship between the initial orientation and the theoretical ET. Forty percent, 77%, and 94% of observed ETs were within the top 10%, 25%, and 40% quantiles, respectively (0.1, 0.25, 0.40 ranking index) of the theoretical ETs (Figs. 4B and S5). In general, the predicted ETs are in line with the observed ones, where the model predicts a multimodal pattern of ET with a higher peak (i.e., optimal ET) at the maximum T_{diff} ($T_{diff,1}$) and a second lower peak (i.e., suboptimal ET) at the second local maximum of T_{diff} ($T_{diff,2}$). When the initial orientation is <20° (Figs. 4A; β =15°, 4B and 5B), the optimal and suboptimal ETs are around 100° (away response) and −100° (toward response), respectively, which is consistent with the bimodal distribution of our experiment (Fig. 2A; $0° \leq \beta < 30°$). At initial orientations in the range 20–60°, the suboptimal ET switches from around −100° to 170° (Figs. 4A; β =45°, 4B and 5B), although

236 $T_{diff,2}$ is extremely small compared to $T_{diff,1}$ (Figs. 4A; β =45°, 4B and 5B). Accordingly, the second
237 peak (i.e., at around 170°) was negligible in our experimental data (Fig. 2A; 30°≤β <60°), even though
238 the fish can potentially reach such an ET (i.e., from such an initial orientation, an 170° ET is within
239 the upper limit of |α|, 147°). When the initial orientation is 60–120° (Figs. 4A; β =75° and β =105°, 4B
240 and 5B), the optimal ET is 100–140° (gradually shifting from 100° to 140°), and the suboptimal ET is
241 around 170°. These two peaks and the shift of the optimal ET are consistent with the experimental
242 results (Fig. 2A; 60°≤β<90° and 90°≤β<120°). The values of the optimal and suboptimal ETs are
243 reversed at initial orientations >120° (Figs. 4B and 5B), as the optimal and suboptimal values become
244 170–180° and around 140°, respectively (Fig. 4A). These results are again consistent with the bimodal
245 distribution of our experiments (Fig. 2A; 120°≤β<150° and 150°≤β≤180°).

246 Figure 4C shows the circular histogram of the overall theoretical ETs estimated by Monte
247 Carlo simulation. The theoretical ETs show two large peaks at around 110–130° and 170–180°, and
248 one small peak at around −100° (Fig. 4C). This theoretically estimated ET distribution is similar to the
249 frequency distribution of the observed ETs (Fig. 2C); there were no significant differences in the
250 frequency distribution between theoretical and observed ETs in 986 of 1000 simulations (Table 2; two-
251 sample Kuiper test, median V=0.10, median P=0.63).

252 To investigate how the initial orientation of the prey modulates the proportion of using the
253 theoretically optimal ET (i.e., where T_{diff} is the maximum, $T_{diff,1}$) compared to using the suboptimal ET
254 (i.e., where T_{diff} is the second local maximum, $T_{diff,2}$), we calculated the optimal ET advantage

255 ($T_{diff,1}-T_{diff,2}$) (Fig. 5A), which represents the difference in the buffer time available for the prey to
256 escape from the predator, at different initial orientations. The fish chose the optimal and suboptimal
257 ETs to a similar extent when the optimal ET advantage is negligible (Fig. 5C). For example, when
258 looking at the optimal ET advantage <2 ms, where the initial orientation is 0–7° and 106–180° (46%
259 of all initial orientations), the proportion of the optimal ET used was only 55% (Fig. 5B and C). On
260 the other hand, the proportion of the optimal ET used was 78% when the optimal ET advantage is
261 higher than 5 ms (i.e., when the initial orientation is 17–82°) (Fig. 5B and C). There was a significant
262 effect of optimal ET advantage on the proportion of the optimal ET used by fish tested in our
263 experiments (Mixed-effects logistic regression analysis, χ^2 =11.06, P<0.01).

264 To investigate the effects of two factors [i.e., the endpoint of the predator attack D_{attack} and the
265 time required for the prey to turn $T_1(|\alpha|)$] on the predictions of ET separately, we constructed three
266 additional geometrical models (Figs. S6–S8): a model that includes only D_{attack}, a model that includes
267 only $T_1(|\alpha|)$, and a null model that includes neither factors (Fig. 1A and ref. 15). In all of these models,
268 the theoretical ET distributions estimated through Monte Carlo simulations were significantly different
269 from the observed ET distributions (Table 2; two-sample Kuiper test, median P<0.01). The null model
270 and the model with $T_1(|\alpha|)$ show unimodal patterns of ET distribution (Figs. S7 and S8). Although the
271 model with D_{attack} shows a multimodal pattern of ET distribution, the simulation based on this model
272 does not match the experimental data, likely because of differences in the relative heights of the peaks
273 (Fig. S6).

Discussion

Our geometrical model, incorporating the endpoint of the predator attack, D_{attack}, and the time required for the prey to turn, $T_1(|\alpha|)$, to maximize the difference between the prey and the predator in the time of arrival at the edge of the safety zone, T_{diff}, clearly explains the multimodal patterns of ETs in *P. major*. Figure 6 shows an example of how multiple ETs result in successful escapes from predators. Specifically, according to the model, when the prey escapes at 140° or 170°, it will not be captured by the predator. On the other hand, when the prey escapes along an intermediate trajectory (157°), it will be captured because it swims toward the corner of the rectangular danger zone to exit it, and therefore it needs to travel a longer distance than when escaping at 140° or 170°. This example illustrates that the multimodal patterns of ETs are likely to be attributable to the existence of two escape routes: either moving sideways to depart from the predator's strike path or moving away from the predator to outrun it. Interestingly, both components of the predator-prey interaction [i.e., D_{attack} and $T_1(|\alpha|)$] added to the previous model (15) are important for accurate predictions of the ET distribution because when they are considered by the model separately, the predictions do not match the experimental data (Figs. S6 and S7; Table 2).

Two different escape tactics have been proposed to enhance the success of predator evasion: the optimal tactic, which maximizes T_{diff} (i.e., the distance between the prey and the predator) (4, 14, 15), and the protean tactic, which maximizes unpredictability to prevent predators from adjusting their

strike trajectories accordingly (19-21, 35). Our results suggest that the prey combines these two different tactics by using multiple preferred ETs. Specifically, when the optimal ET advantage is large (i.e., when the initial orientation is 20–60°), the prey mainly uses the optimal ET (Figs. 2A and 5). However, when the optimal ET advantage over the suboptimal ET is negligible (i.e., the initial orientation is close to 0° or within the range 110–180°), the prey uses optimal and suboptimal ETs to a similar extent (Figs. 2A and 5). In such cases, the escape trajectory of the prey would be highly unpredictable for the predator. While the unpredictability at initial orientations near 0° and 180° can be easily explained by the left-right indecision at orientations nearly perpendicular to the threat (18, 33, 36), yielding ETs that are approximately symmetrical to the axis of the predator attack, the unpredictability observed at initial orientations near 110–180° is related to the similarly advantageous choice between escaping with an ET at around 140° or 180°. Interestingly, at initial orientations >120°, our results show that these two ETs are reached by using toward and away responses, respectively. The overlap between the ETs of toward and away responses in the overall dataset (Fig. 2) suggests that toward responses are not "tactical mistakes" of the prey that turns toward a threat, but are simply related to reaching an optimal or suboptimal ET. These results suggest that the prey strategically adjusts the use of optimal and protean tactics based on their initial orientation. This allows the prey to have unpredictable ETs, thereby preventing predators from anticipating their escape behavior, while keeping T_{diff} large enough to enter the safety zone before the predator reaches it.

A relevant question from a perspective of neurosensory physiology is how the animals are

312 able to determine their ETs within milliseconds of response time. The initial orientation of the prey has
313 been incorporated into various neural circuit models (37-40), but these models assume that prey
314 animals always escape toward 180° (i.e., opposite to the stimulus source), irrespective of the initial
315 orientation. However, the present study shows that animals use suboptimal ETs as well as optimal ETs,
316 and that these ETs may change in a nonlinear fashion, depending on the initial orientation. Thus, we
317 require new neurophysiological models of ETs to understand how neural circuits process the sensory
318 cues of a threatening stimulus, resulting in muscle actions that generate multiple preferred ETs.

319 Our geometrical model assumes that the prey determines the ETs based on a fixed predator
320 speed. This assumption is supported by the results of our experiments, where the effects of predator
321 speed on the mean and variability of ETs are not significant. Although we did not find any effect of
322 predator speed, it is possible that a speed outside the range we used may affect ETs. Recent studies
323 show that larval zebrafish *Danio rerio* exhibit less variable ETs under faster threats than they do under
324 slower threats (41, 42), and the difference in ET variability between fast and slow threats is dependent
325 on whether the Mauthner cell is active or not (42). Therefore, any differences in the ET variability of
326 the present study compared to previous studies could be related to the different involvement of the
327 Mauthner-cells. Using the conventional geometrical model, Soto *et al.* (14) showed that the choice of
328 ET only matters to a prey when the predator speed is intermediate, because a prey that is much faster
329 than its predator can escape by a broad range of ETs, whereas a prey that is much slower than its
330 predator cannot escape by any ETs (43). The predator speed used in this study is in the range of the

real predator speed in the previous study using the same species of both predator and prey (12). Thus, our results are ecologically relevant, and the prey is likely to have optimized their ETs based on a fixed predator speed, where the choice of ET strongly affects their survival.

The relationship between $|\alpha|$ and the time required for a 15-mm displacement, $T_1(|\alpha|)$, (Fig. 3A) indicates that the time required for a 15-mm displacement is relatively constant up to an $|\alpha|$ of about 45°, while a further change in $|\alpha|$ requires additional time. This relationship is likely to be attributable to the kinematics and hydrodynamics of the C-start escape response, because the initial velocity after the stage 1 turn increases linearly up to about 45°, beyond which it plateaus (Fig. 3B). Interestingly, a recent study on swimming efficiency during acceleration found that efficiency increases linearly with yaw amplitudes up to a certain value, beyond which efficiency plateaus (44).

Our geometrical model may be applicable to ETs in other predator-prey systems. The model assumes that the predator makes an in-line attack toward the prey with a limited attack distance. This assumption is likely to be met in attacks by ambush and stalk-and-attack predators (45), such as frogs (11), spiders (13), and many fish species (12, 22, 23, 46). Conversely, some predators adjust their strike direction before and/or during the attack (47-50). Such cases probably violate the model assumption and might be better modeled by a different predator movement (50, 51). Further empirical measurements of both prey and predator movements should be accumulated to confirm whether and in which cases our model accurately describes real predator-prey behaviors.

Our results represent a major advancement in understanding the basis of the variability in ETs

observed in previous works (reviewed in ref. 16). Our results suggest that prey use multiple preferred ETs to maximize the time difference between itself and the attacking predator, while keeping a high level of unpredictability. The results also suggest that prey strategically adjust the use of protean and optimal tactics with respect to the advantage of the optimal ET over the suboptimal ET. Because multimodal ETs similar to what we observed here have been found in many fish species and other animal taxa (16), this behavioral phenotype may result from convergent evolution in phylogenetically distant animals. From a neurosensory perspective, our findings open new avenues to investigate how the animals determine their ETs from multiple options with specific probabilities, which are modulated by the initial orientation with respect to the threat.

Materials and Methods

Definition of the Angles

The C-start escape response consists of an initial bend (stage 1), followed by a return tail flip (stage 2), and continuous swimming or coasting (stage 3) (30, 31). In line with previous studies (16, 33, 52), we defined directionality (away or toward responses), initial orientation β, turn angle α, and ET $\alpha+\beta$ as follows (Fig. S1). *Directionality*: the away and toward responses were defined by the first detectable movement of the fish in a direction either away from or toward the predator, respectively (16). *Initial orientation* (β): the angle between the line passing through the prey's center of mass [CoM; located at

369 34% of the total length from the tip of the snout (12)] and the tip of the snout at the onset of stage 1,
370 and the midline of the predator model attacking in a straight line. Initial orientation ranges from 0°
371 (i.e., when the prey is attacked from front) to 180° (i.e., when the prey is attacked from behind). *Turn*
372 *angle* (α): the angle between the line passing through the CoM and the tip of the snout at the onset of
373 stage 1, and the line passing through the CoM at the onset of stage 1 and the CoM at the end of stage
374 2. The angles of the away and toward responses are assigned positive and negative values, respectively.
375 *ET* ($\alpha+\beta$): the sum of the initial orientation (β) and the turn angle (α). ET is a circular variable since it
376 can span 360°. Because the experimental data exhibited no asymmetry in directionality (Fisher's exact
377 test, P=1.00) and ET distribution (two-sample Kuiper test, V=0.14, P=0.61), we pooled the ETs from
378 the left and right sides, treating all fish as though they were attacked from the right side (16).
379
380 **Experiment**
381 We have elicited the escape response of *P. major* [45.33±3.48 mm (mean±s.d.) total length, n=23]
382 using a dummy predator. The experiment was conducted in a plastic tank (540×890×200 mm) filled
383 with seawater to a depth of 80 mm. The water temperature was maintained at 23.8 to 24.7°C. An
384 individual *P. major* was introduced into a PVC pipe (60 mm diameter) set in the center of the tank and
385 acclimated for 15 min. After the acclimation period, the PVC pipe was slowly removed, and the
386 dummy predator, a cast of *Sebastiscus marmoratus* (164 mm in total length and 30 mm in mouth width),
387 was moved toward the *P. major* for a distance of 200 mm by using a plastic rubber band (Fig. S9).

388 Because the previous work shows that *S. marmoratus* attacks *P. major* using a variable speed
389 [1.10±0.65 (0.09-2.31) m s^{-1}, mean±s.d. (range)] (12), we used various strengths of plastic rubber
390 bands to investigate the effect of predator speed on ET. The fish movements were recorded from above,
391 using a high-speed video camera (HAS-L1; Ditect Co., Tokyo, Japan) at 500 frames s^{-1}. Each
392 individual *P. major* was recorded from 5 to 20 times. The recorded videos were analyzed frame by
393 frame using Dipp-Motion Pro 2D (Ditect Co.). The CoM and the tip of the mouth of *P. major* and the
394 tip of the predator's mouth were digitized in each frame to calculate all the kinematic variables. The
395 animal care and experimental procedures were approved by the Animal Care and Use Committee of
396 the Faculty of Fisheries (Permit No. NF-0002), Nagasaki University in accordance with the Guidelines
397 for Animal Experimentation of the Faculty of Fisheries and the Regulations of the Animal Care and
398 Use Committee, Nagasaki University.

399 Because our geometrical model predicts that the initial orientation β and the predator speed
400 U_{pred} affect the ET and turn angle α, we examined these effects by the experimental data using a
401 GAMM with a normal distribution and identity link function (53). ET and α were regarded as objective
402 variables, while predator speed and initial orientation were regarded as explanatory variables and were
403 modeled with a B-spline smoother. Fish ID was regarded as a random factor. Smoothed terms were
404 fitted using penalized regression splines, and the amount of smoothing was determined using the
405 restricted maximum likelihood (REML) method. As was done in previous studies (16, 32, 33), the
406 away and toward responses were analyzed separately. The significance of the initial orientation and

407 predator speed was assessed by the *F*-test. The analysis was conducted using R 3.5.3 (R Foundation
408 for Statistical Computing) with the R package *gamm4*.
409
410 **Parameter Estimation**
411 To predict the relationship between the ET and the relative time difference T_{diff} in each initial
412 orientation by the geometrical model, we obtained D_{width}, D_{attack}, U_{prey}, U_{pred}, and $T_1(|\alpha|)$. D_{width} was
413 regarded as the mouth width of the dummy predator, which was 30 mm. U_{prey} and $T_1(|\alpha|)$ were directly
414 estimated by analyzing the escape responses of the prey. U_{pred} and D_{attack} were optimized by comparing
415 the model outputs with observed ETs.
416
417 Estimation of the Prey's Kinematic Parameters
418 The relationship between $|\alpha|$ and the time required for a displacement of 15 mm, $T_1(|\alpha|)$, was estimated
419 by piecewise linear regression (54). We used piecewise linear regression rather than a commonly used
420 smoothing method such as GAMM, because the smoothing method does not output the timing of the
421 regression change and thus the biological interpretation of the regression curve is problematic (54).
422 The time required for a displacement of 15 mm was regarded as an objective variable, whereas $|\alpha|$ was
423 regarded as an explanatory variable. Fish ID was included as a covariate in order to take into account
424 potential individual differences in the relationship, $T_1(|\alpha|)$. To detect the possible kinematic mechanism
425 of the relationship $T_1(|\alpha|)$, we also examined the relationship between $|\alpha|$ and initial velocity after the

426 stage 1 turn, using piecewise linear regression. Initial velocity after the stage 1 turn was regarded as
427 an objective variable, $|\alpha|$ was regarded as an explanatory variable, and fish ID was included as a
428 covariate. A hierarchical Bayesian model with a Markov chain Monte Carlo (MCMC) method was
429 used to estimate these relationships (54, 55). The number of draws per chain, thinning rate, burn-in
430 length, and number of chains were set as 200000, 1, 100000, and 5, respectively. To test the overall fit
431 of the model, the WAIC of the model was compared with those of the null model (constant) and a
432 simple linear regression model. MCMC was conducted using RStan 2.18.2 (Stan Development Team
433 2019).
434
435 Estimation of Predator speed and Endpoint of the Predator Attack
436 Because we had no previous knowledge about the values of U_{pred} and D_{attack} that the prey regards as
437 dangerous (i.e., the values of U_{pred} and D_{attack} that trigger a response in the prey), we optimized the
438 values using the experimental data in this study. We have input the obtained values of U_{prey}, D_{width}, and
439 $T_1(|\alpha|)$ into the theoretical model. The optimal values were obtained using the ranking index. The ranks
440 of the observed ETs among the theoretical ET choices of 1° increment were standardized as the ranking
441 index, where 0 means that the real fish chose the theoretically optimal ET where T_{diff} is the maximum,
442 and 1 means that the real fish chose the theoretically worst ET where T_{diff} is the minimum. The optimal
443 set of D_{attack} and U_{pred} values was estimated by minimizing the mean ranking index of the observed
444 ETs. The distribution of the optimal ranking index was then fitted to the truncated normal distribution

445 and was used to predict how the fish chose the ETs from the continuum of the theoretically optimal
446 and worst ETs.
447
448 **Model Predictions**
449 We input the above parameters [D_{width}, D_{attack}, U_{prey}, U_{pred}, and $T_1(|\alpha|)$] into the model and calculated
450 how the choice of different ETs affects T_{diff} for each initial orientation β. Because there was a constraint
451 on the possible range of $|\alpha|$ [i.e., fish escaping by C-start have a minimum and maximum $|\alpha|$ (26)], the
452 range of $|\alpha|$ was determined based on its minimum and maximum values observed in our experiment,
453 which were 9~147°.
454 To estimate the overall frequency distribution of ETs that include the data on observed initial
455 orientations, we conducted Monte Carlo simulations. In each observed initial orientation, the ET was
456 chosen from the continuum of the theoretically optimal and worst ETs. The probability of the ET
457 selection was determined by the truncated normal distribution of the optimal ranking index (e.g., the
458 fish could choose theoretically good ETs with higher probability than theoretically bad ETs but the
459 choice is a continuum based on the truncated normal distribution). This process was repeated 1000
460 times to robustly estimate the frequency distribution of the theoretical ETs. In each simulation run, the
461 frequency distribution of the theoretical ETs was compared with that of the observed ETs using the
462 two-sample Kuiper test (56).
463 To investigate how the real prey changes the probability that it uses the theoretically optimal

464 ET or suboptimal ET, we regarded the difference between the maximum of T_{diff} (at the optimal ET)
465 and the second local maximum of T_{diff} (at the suboptimal ET) as the optimal ET advantage, and
466 theoretically estimated the values for all initial orientations. We then examined the relationship
467 between the optimal ET advantage and the proportion of the optimal ET the prey actually chose using
468 a mixed-effects logistic regression analysis (53). Each observed ET was designated as the optimal (1)
469 or the suboptimal (0) based on whether the observed ET was closer to the optimal ET or suboptimal
470 ET. When the prey chose the ET that was more than 35° different from both the optimal and suboptimal
471 ETs, the ET data point was removed from the analysis (these cases were rare: 7%). The choice of ET
472 [optimal (1) or suboptimal (0)] was regarded as an objective variable, while the optimal ET advantage
473 was regarded as an explanatory variable. Fish ID was regarded as a random factor. The significance of
474 the optimal ET advantage was assessed by the likelihood ratio test with χ^2 distribution. The analysis
475 was conducted using R 3.5.3 with the R package *lme4*.

476 To investigate the effects of two factors [i.e., the endpoint of the predator attack D_{attack} and the
477 time required for the prey to turn $T_1(|\alpha|)$] on predictions of ET separately, we compared four
478 geometrical models: the model that includes both D_{attack} and $T_1(|\alpha|)$, the model that includes only D_{attack},
479 the model that includes only $T_1(|\alpha|)$, and the null model. Note that the null model is equivalent to the
480 previous Domenici's model (15). In all models, the values of U_{pred} and D_{attack} were optimized using the
481 ranking index. The overall frequency distributions of ETs were estimated through Monte Carlo

simulations, and in each simulation run, the theoretical ET distribution was compared with the observed ET distribution using the two-sample Kuiper test.

ACKNOWLEDGMENTS. We sincerely thank Y. Watanabe for his constructive comments on an early version of this paper. This study was funded by Grants-in-Aid for Scientific Research, Japan Society for the Promotion of Science, to Y.K. (17K17949 and 19H04936), Sumitomo Foundation to Y.K. (153128), and the ISM Cooperative Research Program to Y.K. and K.S (2014-ISM.CRP-2006).

References

1. T. H. Bullock, "Comparative neuroethology of startle, rapid escape, and giant fiber-mediated responses" in Neural mechanisms of startle behavior. (Springer, 1984), pp. 1-13.
2. W. Cooper, D. T. Blumstein, *Escaping from predators* (Cambridge University Press, Cambridge, 2015), pp. 442.
3. J. J. Meager, P. Domenici, A. Shingles, A. C. Utne-Palm, Escape responses in juvenile Atlantic cod *Gadus morhua* L.: the effects of turbidity and predator speed. *J. Exp. Biol.* **209**, 4174-4184 (2006).
4. S. A. Arnott, D. M. Neil, A. D. Ansell, Escape trajectories of the brown shrimp *Crangon crangon*, and a theoretical consideration of initial escape angles from predators. *J. Exp. Biol.* **202**, 193-209 (1999).
5. P. W. Bateman, P. A. Fleming, Switching to Plan B: Changes in the escape tactics of two grasshopper species (Acrididae: Orthoptera) in response to repeated predatory approaches. *Behav. Ecol. Sociobiol.* **68**, 457-465 (2014).
6. A. M. Hein, M. A. Gil, C. R. Twomey, I. D. Couzin, S. A. Levin, Conserved behavioral circuits govern high-speed decision-making in wild fish shoals. *Proc. Natl. Acad. Sci. USA* **115**, 12224-12228 (2018).
7. M. Broom, G. D. Ruxton, You can run - or you can hide: Optimal strategies for cryptic prey against pursuit predators. *Behav. Ecol.* **16**, 534-540 (2005).
8. W. E. Cooper, Jr. *et al.*, Effects of risk, cost, and their interaction on optimal escape by nonrefuging Bonaire whiptail lizards, *Cnemidophorus murinus*. *Behav. Ecol.* **14**, 288-293 (2003).
9. J. A. Walker, C. K. Ghalambor, O. L. Griset, D. McKenney, D. N. Reznick, Do faster starts increase the probability of evading predators? *Funct. Ecol.* **19**, 808-815 (2005).
10. E. Shifferman, D. Eilam, Movement and direction of movement of a simulated prey affect the

success rate in barn owl *Tyto alba* attack. *J. Avian Biol.* **35**, 111-116 (2004).

11. J. M. Camhi, W. Tom, S. Volman, The escape behavior of the cockroach *Periplaneta americana*- II. Detection of natural predators by air displacement. *J. Comp. Physiol. A Sens. Neural Behav. Physiol.* **128**, 203-212 (1978).
12. H. Kimura, Y. Kawabata, Effect of initial body orientation on escape probability of prey fish escaping from predators. *Biol. Open* **7**, bio023812 (2018).
13. O. Dangles, N. Ory, T. Steinmann, J. P. Christides, J. Casas, Spider's attack versus cricket's escape: velocity modes determine success. *Anim. Behav.* **72**, 603-610 (2006).
14. D. Weihs, P. W. Webb, Optimal avoidance and evasion tactics in predator-prey interactions. *J. Theor. Biol.* **106**, 189-206 (1984).
15. P. Domenici, The visually mediated escape response in fish: predicting prey responsiveness and the locomotor behaviour of predators and prey. *Mar. Freshwat. Behav. Physiol.* **35**, 87-110 (2002).
16. P. Domenici, J. M. Blagburn, J. P. Bacon, Animal escapology II: Escape trajectory case studies. *J. Exp. Biol.* **214**, 2474-2494 (2011).
17. W. E. Cooper, Risk factors and escape strategy in the grasshopper *Dissosteira carolina*. *Behaviour* **143**, 1201-1218 (2006).
18. P. Domenici, R. W. Blake, Escape trajectories in angelfish (*Pterophyllum eimekei*). *J. Exp. Biol.* **177**, 253-272 (1993).
19. P. Domenici, J. M. Blagburn, J. P. Bacon, Animal escapology I: Theoretical issues and emerging trends in escape trajectories. *J. Exp. Biol.* **214**, 2463-2473 (2011).
20. D. A. Humphries, P. M. Driver, Protean defence by prey animals. *Oecologia* **5**, 285-302 (1970).
21. K. A. Jones, A. L. Jackson, G. D. Ruxton, Prey jitters; protean behaviour in grouped prey. *Behav. Ecol.* **22**, 831-836 (2011).
22. P. W. Webb, J. M. Skadsen, Strike tactics of *Esox*. *Can. J. Zool.* **58**, 1462-1469 (1980).
23. W. R. Fouts, D. R. Nelson, Prey capture by the pacific angel shark, *Squatina californica*: visually mediated strikes and ambush-site characteristics. *Copeia* **1999**, 304-312 (1999).
24. C. W. Anderson, The modulation of feeding behavior in response to prey type in the frog *Rana pipiens*. *J. Exp. Biol.* **179**, 1-12 (1993).
25. A. Paglianti, P. Domenici, The effect of size on the timing of visually mediated escape behaviour in staghorn sculpin *Leptocottus armatus*. *J. Fish Biol.* **68**, 1177-1191 (2006).
26. P. Domenici, R. W. Blake, The kinematics and performance of the escape response in the angelfish (*Pterophyllum eimekei*). *J. Exp. Biol.* **156**, 187-205 (1991).
27. N. Danos, G. V. Lauder, Challenging zebrafish escape responses by increasing water viscosity. *J. Exp. Biol.* **215**, 1854-1862 (2012).
28. M. Fleuren *et al.*, Three-dimensional analysis of the fast-start escape response of the least killifish, *Heterandria formosa*. *J. Exp. Biol.* **221** (2018).
29. D. J. Ellerby, J. D. Altringham, Spatial variation in fast muscle function of the rainbow trout *Oncorhynchus mykiss* during fast-starts and sprinting. *J. Exp. Biol.* **204**, 2239-2250 (2001).

30. P. Domenici, R. W. Blake, The kinematics and performance of fish fast-start swimming. *J. Exp. Biol.* **200**, 1165-1178 (1997).
31. D. Weihs, The mechanism of rapid starting of slender fish. *Biorheology* **10**, 343-350 (1973).
32. P. Domenici, D. Booth, J. M. Blagburn, J. P. Bacon, Escaping away from and towards a threat: The cockroach's strategy for staying alive. *Communicative and Integrative Biology* **2**, 497-500 (2009).
33. A. Nair, K. Changsing, W. J. Stewart, M. J. McHenry, Fish prey change strategy with the direction of a threat. *Proc. R. Soc. Lond. B* **284** (2017).
34. P. Domenici, D. Booth, J. M. Blagburn, J. P. Bacon, Cockroaches keep predators guessing by using preferred escape trajectories. *Curr. Biol.* **18**, 1792-1796 (2008).
35. R. H. J. M. Kurvers *et al.*, The evolution of lateralization in group hunting sailfish. *Curr. Biol.* **27**, 521-526 (2017).
36. P. Domenici, R. S. Batty, Escape behaviour of solitary herring (*Clupea harengus*) and comparisons with schooling individuals. *Mar. Biol.* **128**, 29-38 (1997).
37. R. C. Eaton, R. K. K. Lee, M. B. Foreman, The Mauthner cell and other identified neurons of the brainstem escape network of fish. *Prog. Neurobiol.* **63**, 467-485 (2001).
38. O. Yono, T. Shimozawa, Synchronous firing by specific pairs of cercal giant interneurons in crickets encodes wind direction. *Biosystems* **93**, 218-225 (2008).
39. G. M. Card, Escape behaviors in insects. *Curr. Opin. Neurobiol.* **22**, 180-186 (2012).
40. R. Levi, J. M. Camhi, Population vector coding by the giant interneurons of the cockroach. *J. Neurosci.* **20**, 3822-3829 (2000).
41. W. J. Stewart, A. Nair, H. Jiang, M. J. McHenry, Prey fish escape by sensing the bow wave of a predator. *J. Exp. Biol.* **217**, 4328-4336 (2014).
42. K. Bhattacharyya, D. L. McLean, M. A. MacIver, Visual threat assessment and reticulospinal encoding of calibrated responses in larval zebrafish. *Curr. Biol.* **27**, 2751-2762 e2756 (2017).
43. A. Soto, W. J. Stewart, M. J. McHenry, When optimal strategy matters to prey fish. *Integr. Comp. Biol.* **55**, 110-120 (2015).
44. O. Akanyeti *et al.*, Accelerating fishes increase propulsive efficiency by modulating vortex ring geometry. *Proc. Natl. Acad. Sci. USA* **114**, 13828-13833 (2017).
45. T. Y. Moore, A. A. Biewener, Outrun or outmaneuver: predator–prey interactions as a model system for integrating biomechanical studies in a broader ecological and evolutionary context. *Integr. Comp. Biol.* **55**, 1188-1197 (2015).
46. D. M. Rand, G. V. Lauder, Prey capture in the chain pickerel, *Esox niger*: correlations between feeding and locomotor behavior. *Can. J. Zool.* **59**, 1072-1078 (1981).
47. R. Olberg, A. Worthington, K. Venator, Prey pursuit and interception in dragonflies. *J. Comp. Physiol. A Sens. Neural Behav. Physiol.* **186**, 155-162 (2000).
48. M. J. McHenry *et al.*, The pursuit strategy of predatory bluefish (*Pomatomus saltatrix*). *Proc. R. Soc. Lond. B* **286** (2019).
49. I. Aihara, E. Fujioka, S. Hiryu, Qualitative and quantitative analyses of the echolocation strategies

588 of bats on the basis of mathematical modelling and laboratory experiments. *PLoS ONE* **8** (2013).
589 50. A. J. Corcoran, W. E. Conner, How moths escape bats: predicting outcomes of predator-prey
590 interactions. *J. Exp. Biol.* **219**, 2704-2715 (2016).
591 51. H. C. Howland, Optimal strategies for predator avoidance: The relative importance of speed and
592 manoeuvrability. *J. Theor. Biol.* **47**, 333-350 (1974).
593 52. W. J. Stewart, G. S. Cardenas, M. J. McHenry, Zebrafish larvae evade predators by sensing water
594 flow. *J. Exp. Biol.* **216**, 388-398 (2013).
595 53. A. Zuur, E. N. Ieno, N. Walker, A. A. Saveliev, G. M. Smith, *Mixed effects models and extensions in*
596 *ecology with R* (Springer, New York, 2009), pp. 574.
597 54. S. L. Brilleman, L. D. Howe, R. Wolfe, K. Tilling, Bayesian piecewise linear mixed models with a
598 random change point: an application to BMI rebound in childhood. *Epidemiology* **28**, 827-833
599 (2017).
600 55. M. Kéry, M. Schaub, *Bayesian population analysis using winbugs – a hierarchical perspective*
601 (Academic Press, Burlington, 2011), pp. 535.
602 56. J. H. Zar, *Biostatistical analysis: fifth edition* (Pearson Education, New Jersey, 2010), pp. 944.

603

604

605 Table 1. Widely applicable or Watanabe–Akaike information criterion (WAIC) for each model in the

606 hierarchical Bayesian models

Relationship	WAIC	ΔWAIC
$\lvert\alpha\rvert$–T_1 relationship		
Piecewise linear	1363.7	0
Linear	1376.7	7.0
Constant	1581.1	217.4
$\lvert\alpha\rvert$–initial velocity after stage 1 turn relationship		
Piecewise linear	–218.1	0
Linear	–205.1	13.0
Constant	–171.5	46.6

607 $\lvert\alpha\rvert$, absolute value of the turn angle; T_1, time required for a displacement of 15 mm from the initial

608 position. The best models are shown in bold.

609

610

611 Table 2. Comparison of the distribution of escape trajectories (ETs) between the model prediction and

612 experimental data using the two-sample Kuiper test

Model	Median Kuiper's V	Median P	Rate of $P > 0.05$
With both D_{attack} and $T_1(\|\alpha\|)$	0.10	0.63	0.99
With D_{attack} and without $T_1(\|\alpha\|)$	0.25	< 0.01	0.00
Without D_{attack} and with $T_1(\|\alpha\|)$	0.18	< 0.01	0.13
Neither D_{attack} nor $T_1(\|\alpha\|)$	0.28	< 0.01	0.00

613 D_{attack}, distance between the prey's initial position and the endpoint of the predator attack; $T_1(|\alpha|)$,

614 relationship between the absolute value of the turn angle and the time required for a 15-mm

615 displacement from the initial position (i.e., the time required for the prey to turn).

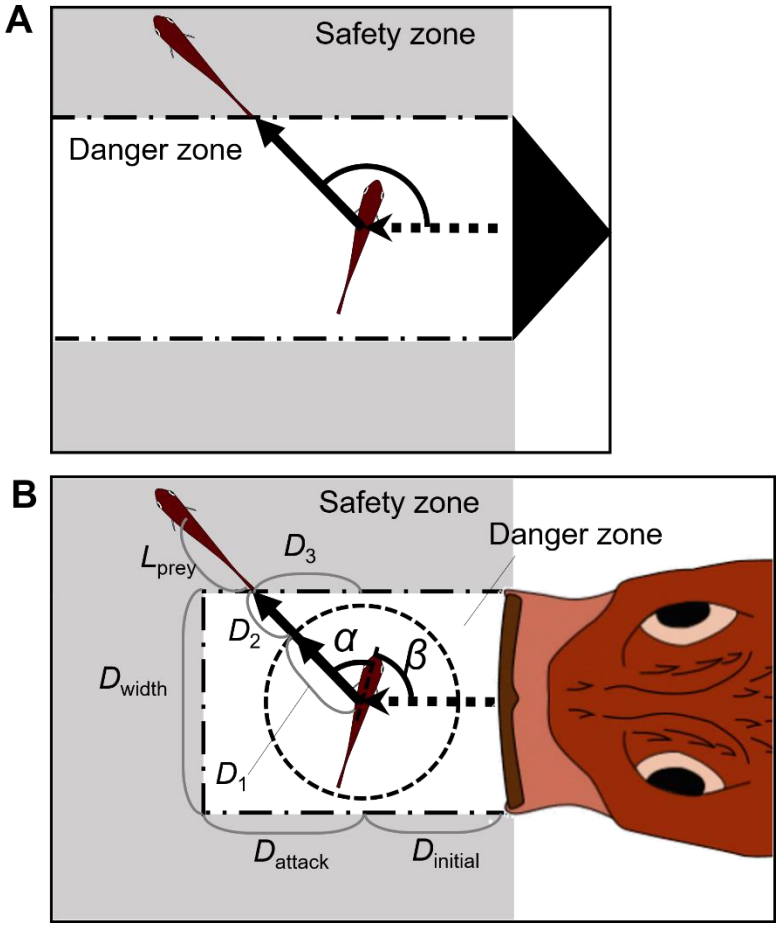

Fig. 1. A proposed geometrical model for animal escape trajectories. (A) A previous geometrical model proposed by Domenici (15). The predation threat with a certain width (the tail of a killer whale, represented by the black triangle) directly approaches the prey, and the prey should reach the safety zone (grey area) outside the danger zone (white area) before the threat reaches that point. In this model, the prey can instantaneously escape in any direction, and the predation threat moves linearly and infinitely. (B) Two factors are added to Domenici's model: the endpoint of the predator attack, and the time required for the prey to turn. See the text for details of the definitions of the variables and mathematical formulas.

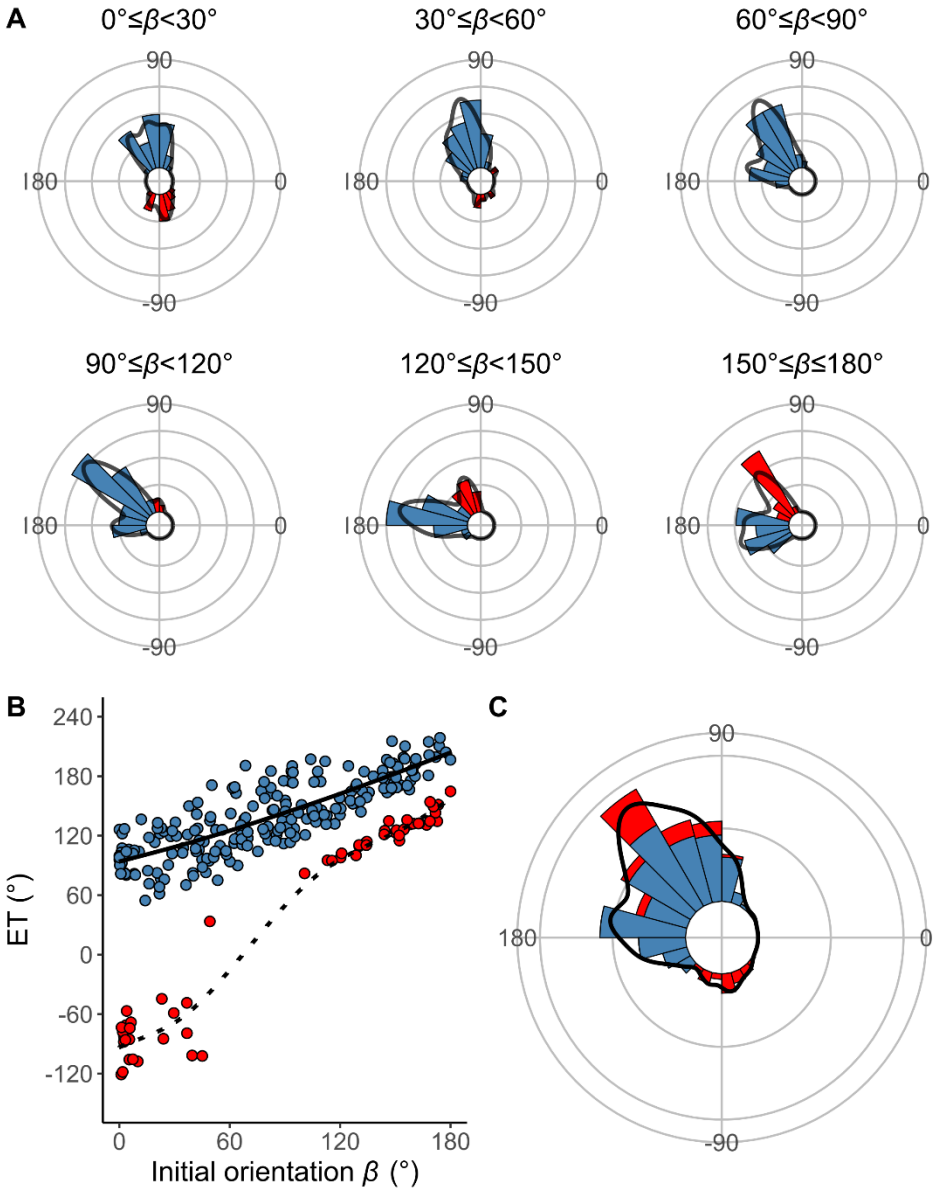

Fig. 2. Results of the experiments of *Pagrus major* attacked by a dummy predator (i.e., a cast of *Sebastiscus marmoratus*). (A) Circular histograms of escape trajectories (ETs) in 30° initial orientation β bins. Solid lines are estimated by the kernel probability density function. Concentric circles represent 5% of the total sample sizes, the bin intervals are 15°, and the bandwidths of the kernel are 50. (B) Relationship between initial orientation and ET. Different colors represent the away (blue) and toward (red) responses. Solid and dotted lines are estimated by the generalized additive mixed model (GAMM). (C) Circular histogram of ETs pooling all the data shown in A. Solid lines are estimated by the kernel probability density function. Concentric circles represent 5% of the total sample sizes, the bin intervals are 15°, and the bandwidths of the kernel are 50. The predator is approaching from the 0° direction.

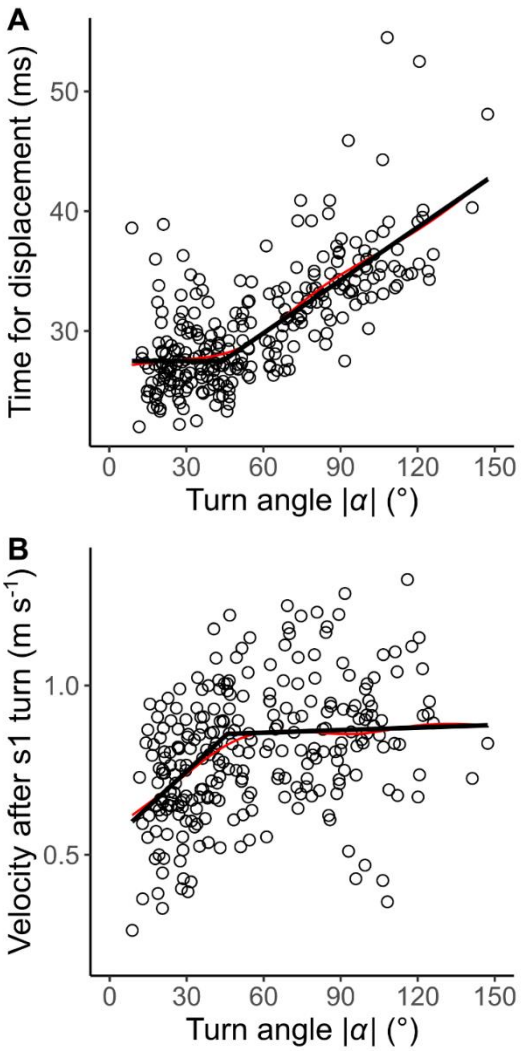

Fig. 3. The relationship between the absolute value of the turn angle $|\alpha|$ and time-distance variables. (A) Relationship between $|\alpha|$ and the time required for a displacement of 15 mm from the initial position of the prey. (B) Relationship between $|\alpha|$ and the initial velocity after stage 1 turn. Solid black lines are estimated by the piecewise linear regression model, and red lines are estimated by the generalized additive mixed model (GAMM).

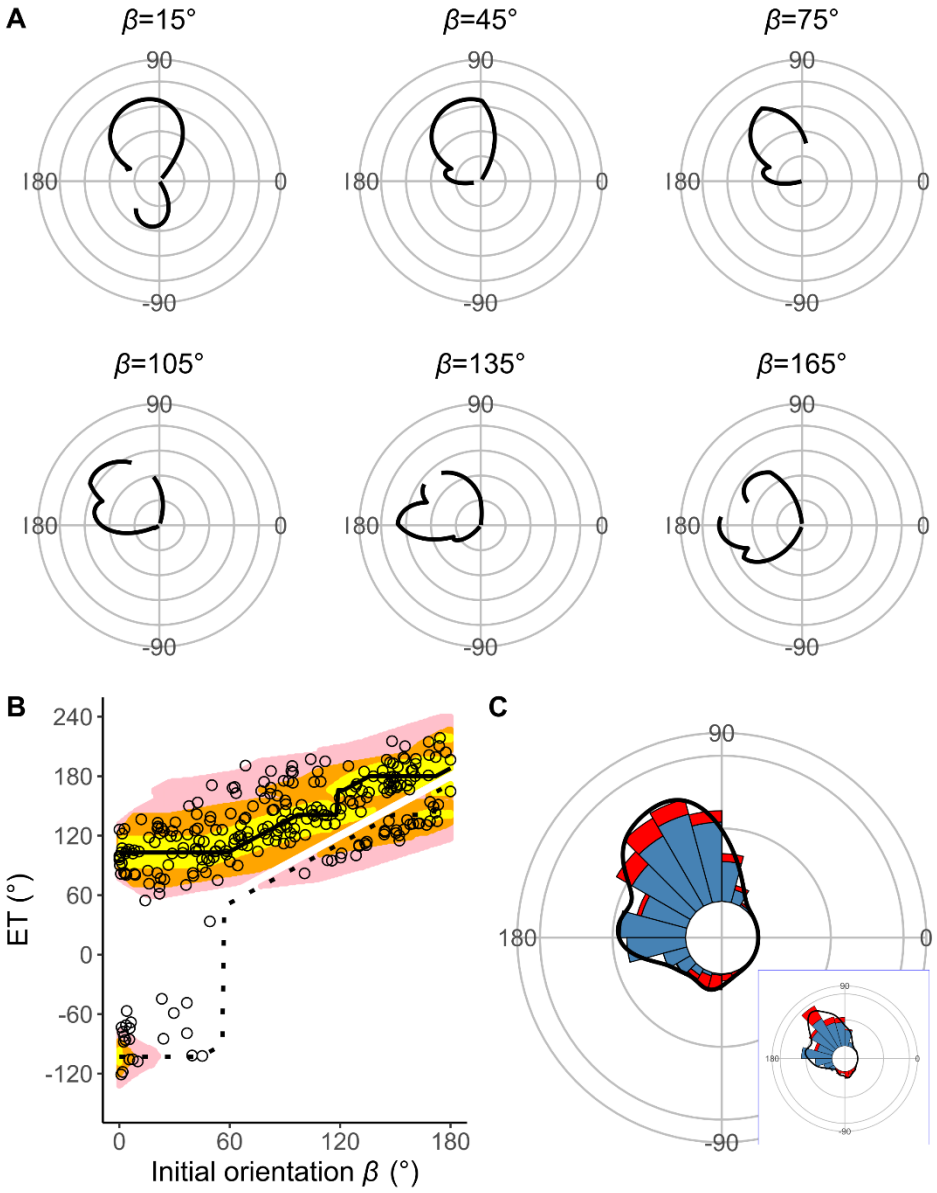

Fig. 4. Model estimates. (A) Circular plots of the time difference between the prey and predator T_{diff} in different initial orientations β. The time difference of the best escape trajectory (ET) was regarded as 10 ms, and the relative time differences between 0 and 10 ms are shown by solid lines. Areas without solid lines indicate that either the time difference is below 0 or the fish cannot reach that ET because of the constraint on the possible range of turn angles $|\alpha|$. Concentric circles represent 3 ms. (B) Relationship between the initial orientation β and ET. Solid and dotted lines represent the best-estimated away and toward responses, respectively. Different colors represent the top 10%, 25%, and 40% quantiles of the time difference between the prey and predator within all possible ETs. (C) Circular histogram of the theoretical ETs, estimated by a Monte Carlo simulation. The probability of selection of an ET was determined by the truncated normal distribution of the optimal ranking index (Fig. S5). This process was repeated 1000 times to estimate the frequency distribution of the theoretical ETs. Colors in the bars represent the away (blue) or toward (red) responses. Black lines represent the kernel probability density function. Concentric circles represent 10 % of the total sample sizes, the bin intervals are 15°, and the bandwidths of the kernel are 50. Circular histogram of the observed ETs (Fig. 2C) is shown in the lower right panel for comparison. The predator is approaching from the 0° direction.

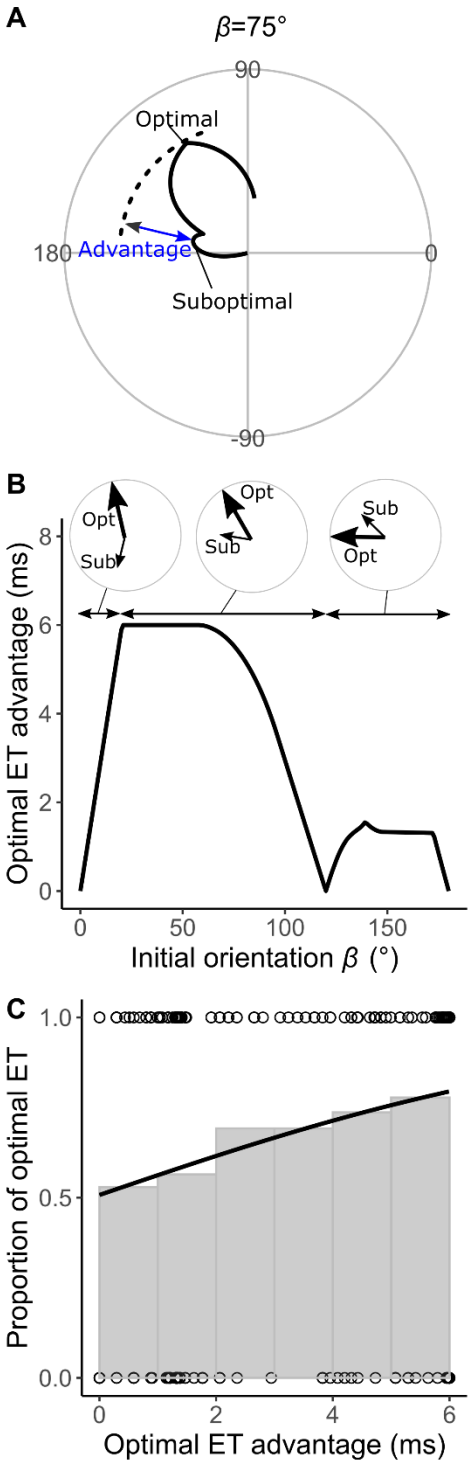

Fig. 5. Analyses of the probability that the prey chooses the optimal vs. suboptimal ETs. (A) The time difference between the prey and predator T_{diff} at the initial orientation β of 75° is shown as an example. We defined the difference between the maximum of T_{diff} (at the optimal ET) and the second local maximum of T_{diff} (at the suboptimal ET) as the optimal ET advantage. (B) Relationship between the initial orientation β and the optimal ET advantage. Large and small arrows in circles represent the optimal and suboptimal ETs, respectively, for each β sectors. (C) Relationship between the optimal ET advantage and the proportion of the optimal ET used by the real prey. Optimal ET and suboptimal ET are designated as 1 and 0, respectively. The line was estimated by the mixed effects logistic regression analysis.

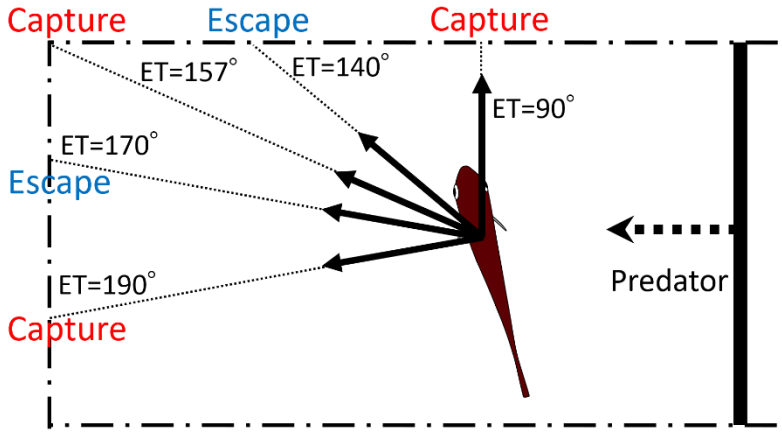

Fig. 6. Schematic drawing showing how multiple escape trajectories (ETs) result in successful escapes from predators. The dash-dotted rectangle represents the danger zone the prey needs to exit in order to escape predation, outside of which is the safety zone. When the prey escapes toward the corner of the rectangular danger zone (ET=157°) to exit it, it needs to travel a relatively long distance and therefore the predator can catch it. On the other hand, when the prey escapes with an ET at 170° or 140°, it covers a shorter distance and can reach the safety zone before the predator's arrival. When the prey escapes with an even smaller ET (90°), it will be captured because the shorter travel distance for the predator overrides the benefits of the smaller turn and shorter travel distance for the prey. When the prey escapes with an even larger ET (190°), it will also be captured, because the prey requires a longer time to turn than if escaping along the 170° ET, whereas the travel distance for both predator and prey is the same as that for the 170° ET. In this example, the initial orientation, flight initiation distance, and the body length posterior to the center of mass were set as 110°, 60 mm and 30 mm, respectively.

Table S1. Akaike information criterion (AIC) for 1–9 Gaussian mixture models to estimate the empirical ET distribution

Number of peaks	AIC	ΔAIC
3	2777.1	0.0
4	2781.0	3.9
2	2784.1	6.9
5	2787.1	10.0
6	2791.1	14.0
7	2797.1	20.0
8	2798.9	21.8
9	2799.2	22.1
1	2855.7	78.6

The best model is shown in bold.

686 Table S2. Widely applicable or Watanabe–Akaike information criterion (WAIC) for each model to estimate
687 the relationship between the absolute value of the turn angle and the time required for a displacement of 10 or
688 20 mm from the initial position

Length of displacement	WAIC	ΔWAIC
10 mm		
Piecewise linear	1239.7	0
Linear	1259.0	19.3
Constant	1524.4	284.7
20 mm		
Piecewise linear	1543.3	0
Linear	1547.0	3.7
Constant	1689.7	146.4

689 The best models are shown in bold.

690 Table S3. Comparison of the distribution of escape trajectories (ETs) between the model prediction and
691 experimental data using the two-sample Kuiper test

Distance for the fast-start phase	Median Kuiper's V	Median P	Rate of $P > 0.05$
10 mm			
With both D_{attack} and $T_1(\|\alpha\|)$	0.10	0.63	0.99
With D_{attack} and without $T_1(\|\alpha\|)$	0.25	< 0.01	0.00
Without D_{attack} and with $T_1(\|\alpha\|)$	0.17	< 0.05	0.25
Neither D_{attack} nor $T_1(\|\alpha\|)$	0.28	< 0.01	0.00
20 mm			
With both D_{attack} and $T_1(\|\alpha\|)$	0.11	0.44	0.96
With D_{attack} and without $T_1(\|\alpha\|)$	0.25	< 0.01	0.00
Without D_{attack} and with $T_1(\|\alpha\|)$	0.15	< 0.05	0.46
Neither D_{attack} nor $T_1(\|\alpha\|)$	0.28	< 0.01	0.00

692 The distance for the fast-start phase was regarded as either 10 or 20 mm. D_{attack}, distance between the prey's
693 initial position and the endpoint of the predator attack; $T_1(|\alpha|)$, relationship between the absolute value of the
694 turn angle and the time required for a 15-mm displacement from the initial position (i.e., the time required for
695 the prey to turn).

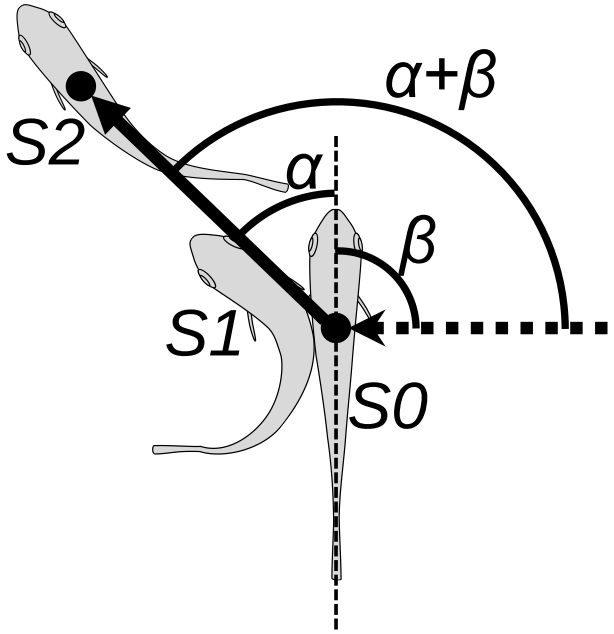

Fig. S1. Schematic drawing of angular variables. *Filled circle* position of the center of mass; *Dotted arrow* approach direction of the dummy predator; *S0* position of the fish at the onset of stage 1, *S1* position at the end of stage 1, *S2* position at the end of stage 2, α turn angle, β initial orientation, $\alpha+\beta$ escape trajectory (ET).

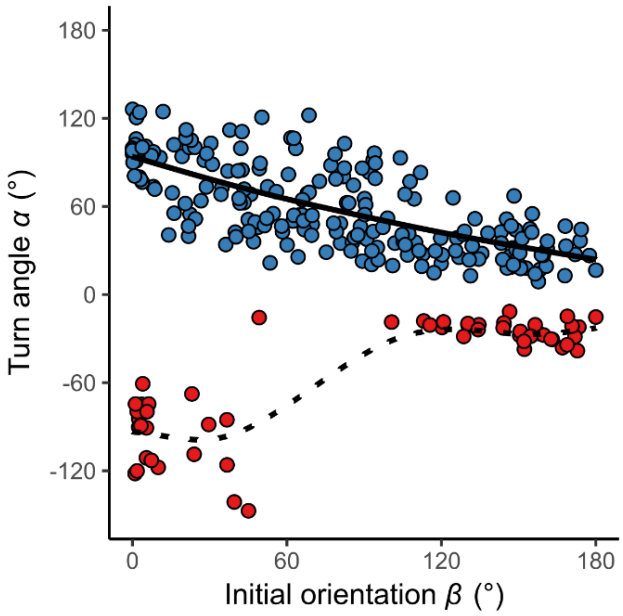

Fig. S2. Relationship between initial orientation β and turn angle α in the experiment. Different colors represent the away (blue) and toward (red) responses. Solid and dotted lines are estimated by the generalized additive mixed model (GAMM).

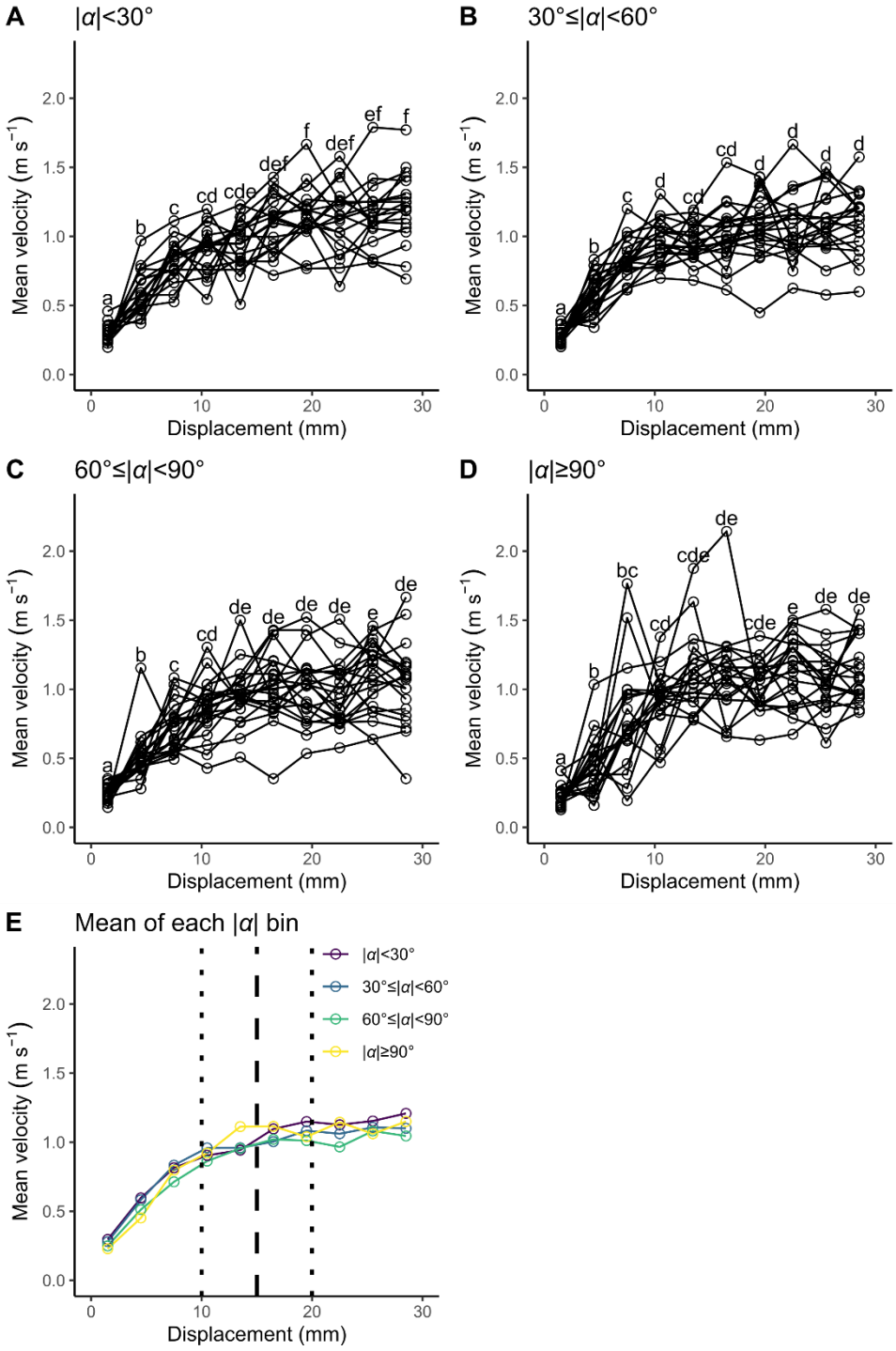

Fig. S3. Relationship between displacement from the initial position (3-mm intervals: 0–3, 3–6, ..., and 27–30 mm) and mean velocity during the displacement for each turn angle ($|\alpha|$) bin. Unfilled circles denote the mean value for each individual. Different lowercase letters represent significant differences according to the paired *t*-test with Bonferroni's correction ($P<0.05$). (A) $|\alpha|<30°$. (B) $30°\leq|\alpha|<60°$. (C) $60°\leq|\alpha|<90°$. (D) $|\alpha|\geq90°$. (E) Mean of the individual mean value for each $|\alpha|$ bin. Vertical dashed line represents the cut-off distance of 15 mm used in this study, and vertical dotted lines represent the other cut-off distances tested in this study (Tables S2 and S3).

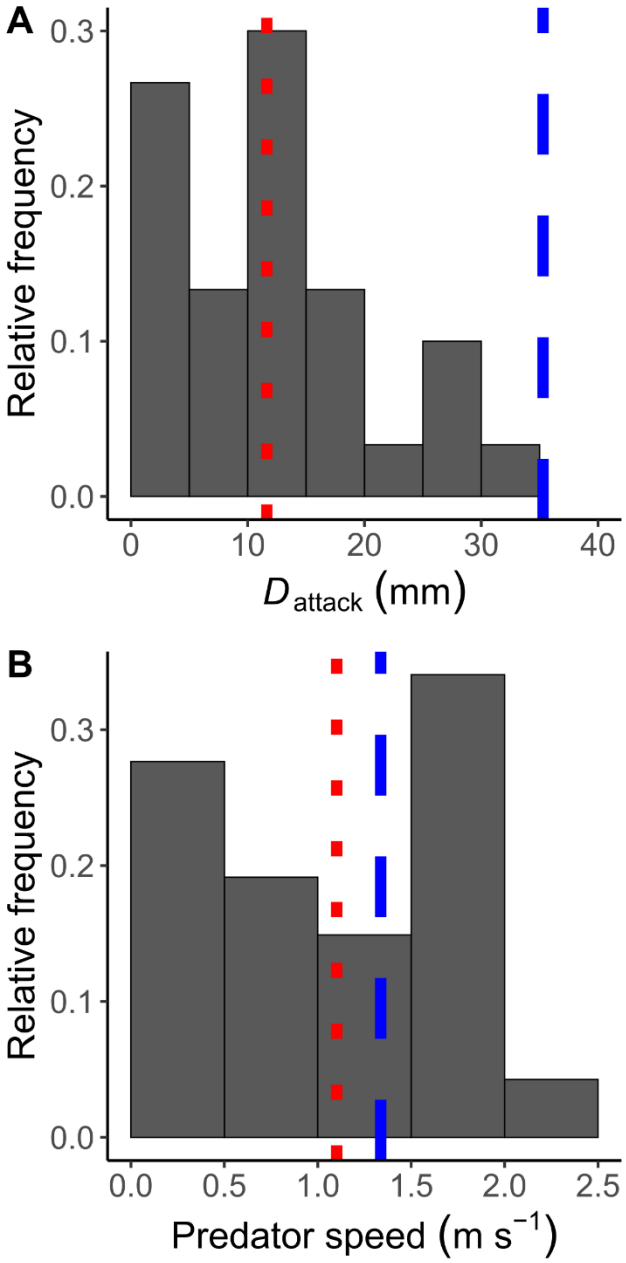

Fig. S4. Predator attack parameters. (A) Histogram of the distance between the prey's initial position and the predator's mouth position at the onset of the mouth closing (D_{attack}). (B) Histogram of the speed of the real predator *Sebastiscus marmoratus*. Both figures are based on reanalysis of data from Kimura and Kawabata (12). Vertical dashed blue lines represent the optimal values independently estimated in this study, and vertical dotted red lines represent the mean values of the real predator.

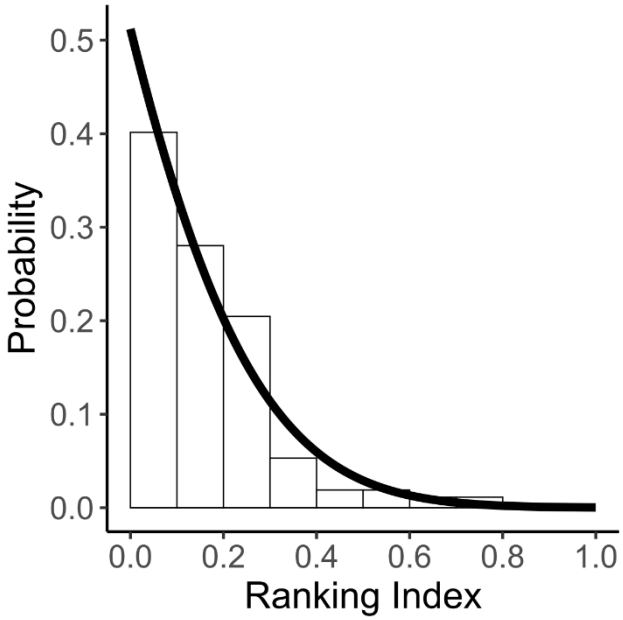

Fig. S5. Histogram of the ranking index, where 0 indicates that the real fish chose the theoretically optimal escape trajectory (ET) and 1 indicates that the real fish chose the theoretically worst ET. The solid line is the density probability function of the truncated normal distribution.

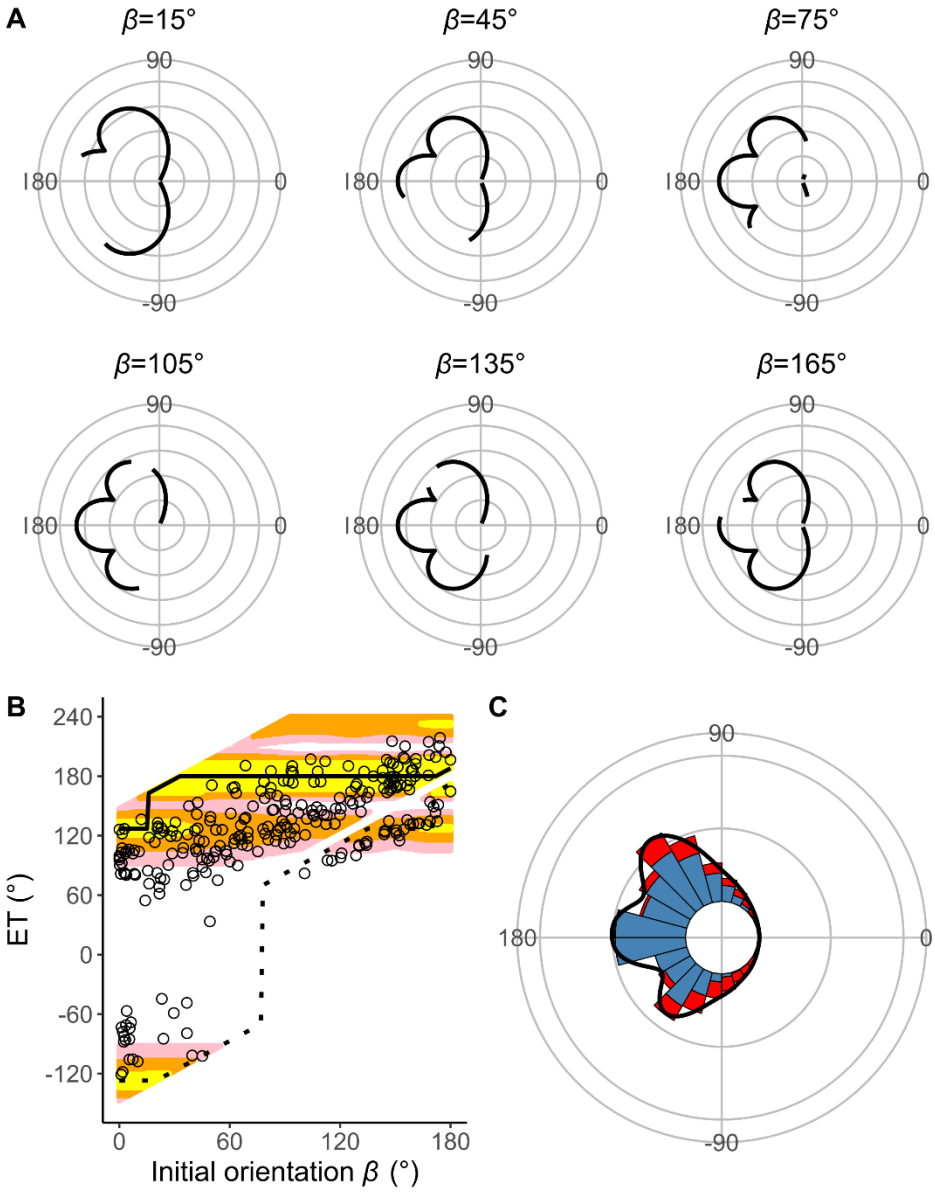

Fig. S6. Estimates of the model with D_{attack} (the distance between the prey's initial position and the endpoint of the predator attack) and without $T_1(|\alpha|)$ (the relationship between the absolute value of the turn angle $|\alpha|$ and the time required for a 15-mm displacement from the initial position, or the time required for prey to turn). (A) Circular plots of the time difference between the prey and predator T_{diff} in different initial orientations β. The time difference of the best escape trajectory (ET) was regarded as 10 ms, and the relative time differences between 0 and 10 ms are shown by solid lines. Areas without solid lines indicate that either the time difference is below 0 or the fish cannot go to that ET because of the constraint on the possible range of $|\alpha|$. Concentric circles represent 3 ms. (B) Relationship between the initial orientation β and ET. Solid and dotted lines represent the best-estimated away and toward responses, respectively. Different colors represent the top 10%, 25%, and 40% quantiles of the time difference between the prey and predator within all possible ETs. (C) Circular histogram of the theoretical ETs, estimated by a Monte Carlo simulation. The probability of selection of an ET was determined by the truncated normal distribution of the optimal ranking index. This process was repeated 1000 times to estimate the frequency distribution of the theoretical ETs. Colors in the bars represent the away (blue) or toward (red) responses. Black lines represent the kernel probability density function. Concentric circles represent 10 % of the total sample sizes, the bin intervals are 15°, and the bandwidths of the kernel are 50. The predator is approaching from the 0° direction.

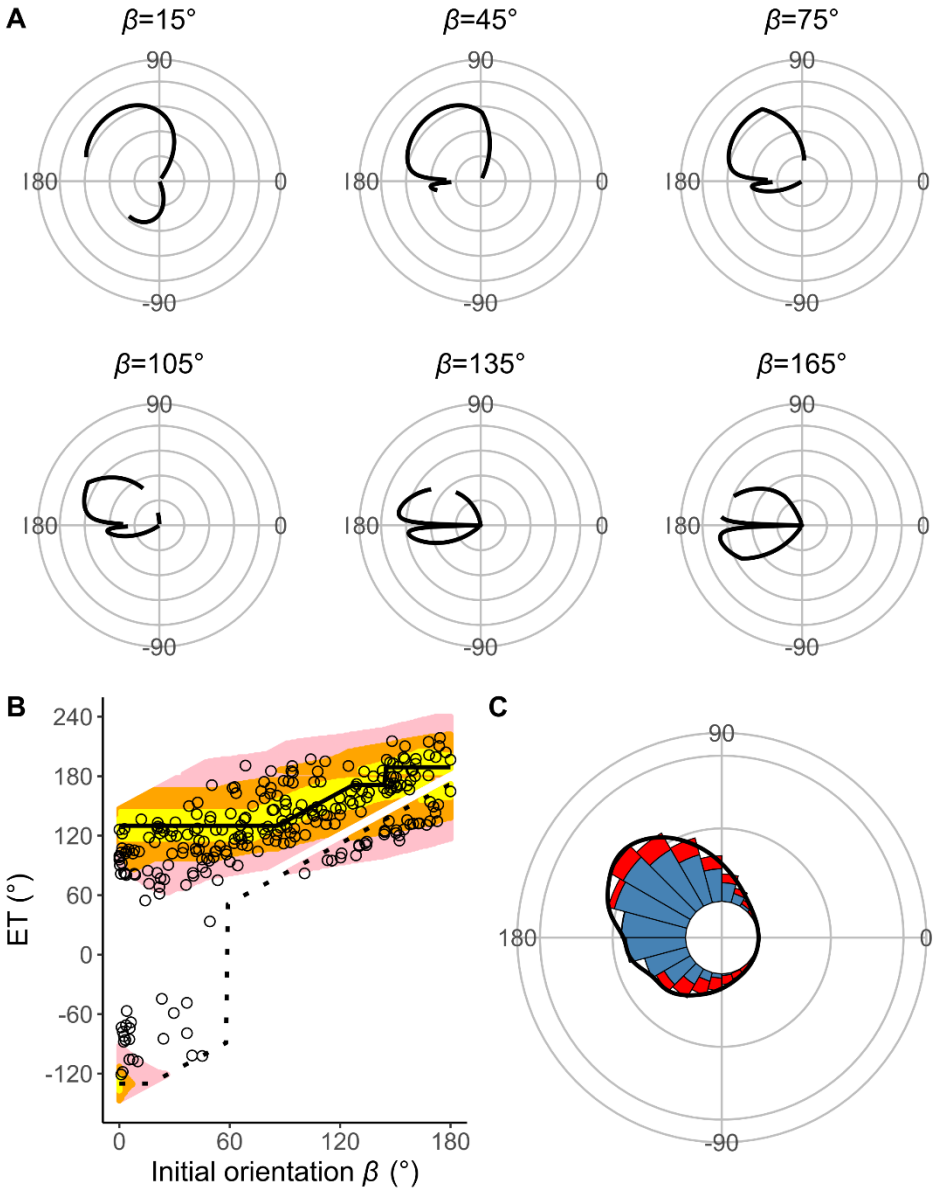

Fig. S7. Estimates of the model with $T_1(|\alpha|)$ (the relationship between the absolute value of the turn angle $|\alpha|$ and the time required for a 15-mm displacement from the initial position, or the time required for the prey to turn) and without D_{attack} (the distance between the prey's initial position and the endpoint of the predator attack). (A) Circular plots of the time difference between the prey and predator T_{diff} in different initial orientations β. The time difference of the best escape trajectory (ET) was regarded as 10 ms, and the relative time differences between 0 and 10 ms are shown by solid lines. Areas without solid lines indicate that either the time difference is below 0 or the fish cannot go to that ET because of the constraint on the possible range of $|\alpha|$. Concentric circles represent 3 ms. (B) Relationship between the initial orientation β and ET. Solid and dotted lines represent the best-estimated away and toward responses, respectively. Different colors represent the top 10%, 25%, and 40% quantiles of the time difference between the prey and predator within all possible ETs. (C) Circular histogram of the theoretical ETs, estimated by a Monte Carlo simulation. The probability of selection of an ET was determined by the truncated normal distribution of the optimal ranking index. This process was repeated 1000 times to estimate the frequency distribution of the theoretical ETs. Colors in the bars represent the away (blue) or toward (red) responses. Black lines represent the kernel probability density function. Concentric circles represent 10 % of the total sample sizes, the bin intervals are 15°, and the bandwidths of the kernel are 50. The predator is approaching from the 0° direction.

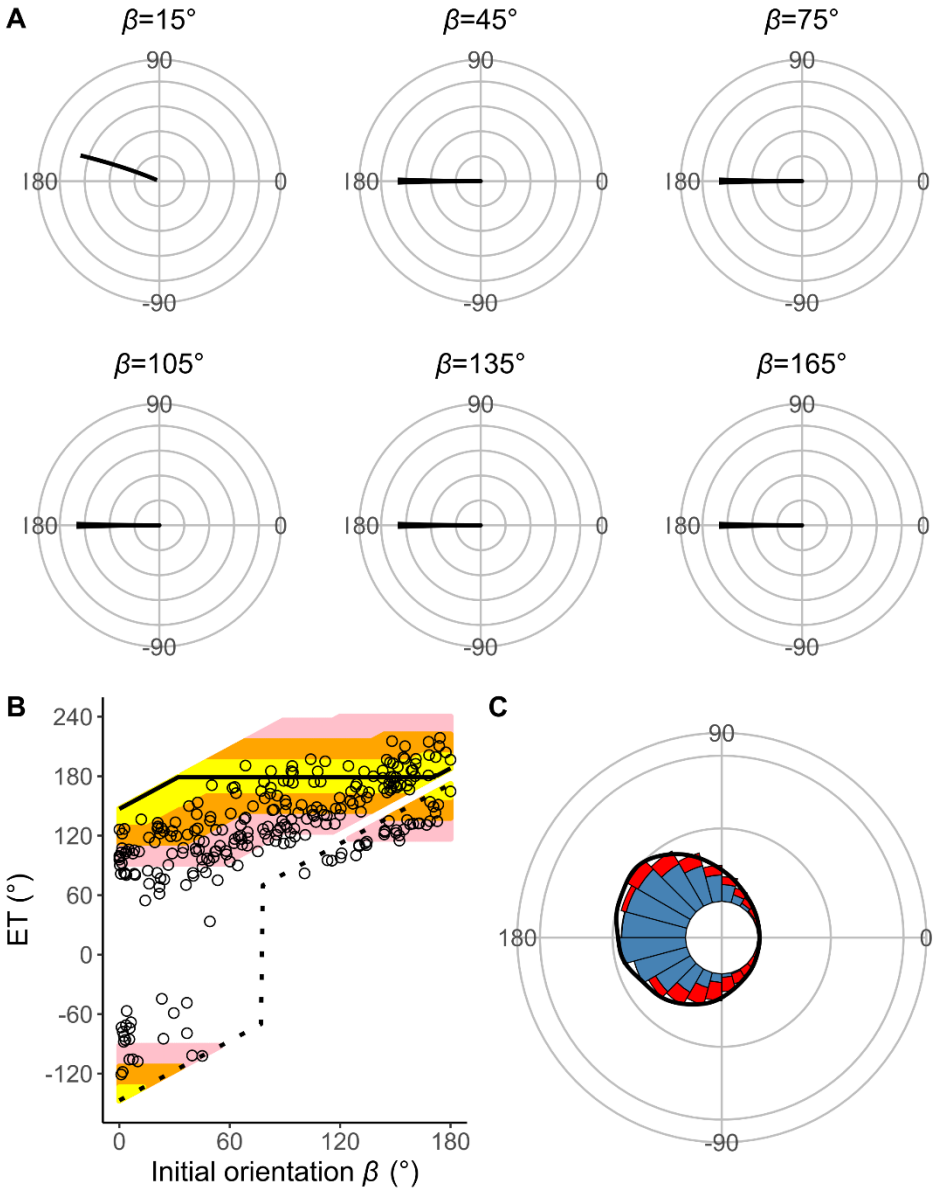

Fig. S8. Estimates of the model that includes neither D_{attack} (the distance between the prey's initial position and the endpoint of the predator attack) nor $T_1(|\alpha|)$ (the relationship between the absolute value of the turn angle $|\alpha|$ and the time required for a 15-mm displacement from the initial position, or the time required for the prey to turn). (A) Circular plots of the time difference between the prey and predator T_{diff} in different initial orientations β. The time difference of the best escape trajectory (ET) was regarded as 10 ms, and the relative time differences between 0 and 10 ms are shown by solid lines. Areas without solid lines indicate that either the time difference is below 0 or the fish cannot go to that ET because of the constraint on the possible range of $|\alpha|$. Concentric circles represent 3 ms. (B) Relationship between the initial orientation β and ET. Solid and dotted lines represent the best-estimated away and toward responses, respectively. Different colors represent the top 10%, 25%, and 40% quantiles of the time difference between the prey and predator within all possible ETs. (C) Circular histogram of the theoretical ETs, estimated by a Monte Carlo simulation. The probability of selection of an ET was determined by the truncated normal distribution of the optimal ranking index. This process was repeated 1000 times to estimate the frequency distribution of the theoretical ETs. Colors in the bars represent the away (blue) or toward (red) responses. Black lines represent the kernel probability density function. Concentric circles represent 10 % of the total sample sizes, the bin intervals are 15°, and the bandwidths of the kernel are 50. The predator is approaching from the 0° direction.

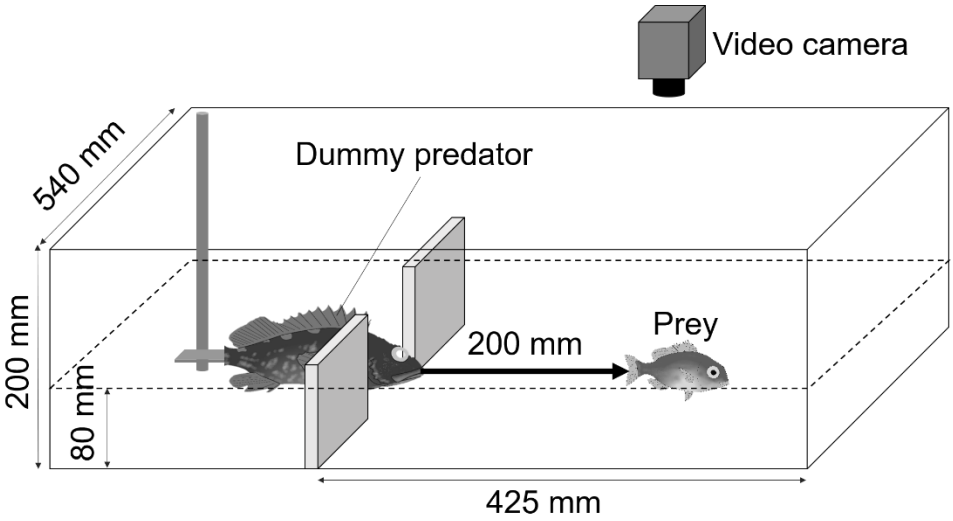

780

781 Fig. S9. Sketch of the experimental apparatus for measuring the escape response of prey fish *Pagrus major*.